Analysis of Waveguides with Metal Inserts

ABBAS S. OMAR, SENIOR MEMBER, IEEE, AND KLAUS F. SCHÜNEMANN, SENIOR MEMBER, IEEE

Abstract—A systematic analysis of waveguides with metal inserts is presented. The method is based on a field expansion in terms of the normal modes of the corresponding hollow waveguide without metal inserts. The analysis leads to two main formulations: the matrix formulation and the moment method formulation. The matrix formulation is suitable for structures with smooth metal inserts, which are free from sharp edges, while the moment method is more suitable for metal sheets (e.g. strips and fins) or metal inserts with sharp edges (e.g. ridges).

The validity of the method is tested by investigating some special cases, in which the surface of the metal insert coincides with one of the coordinate surfaces, e.g. a bifurcation in circular or rectangular waveguides. The method is then applied to the analysis of striplines and ridge waveguides. It leads to a generalization of the widely used spectral-domain technique in that ridges, fins, and strips with finite thickness can now be analyzed likewise. Any existing routine for the analysis of planar structures which is based on the spectral-domain technique can then be slightly modified in order to take the metallization thickness into account.

I. Introduction

MOST OF THE existing methods for the analysis of guiding structures depend to a great extent on the specific geometry of the individual structure. A systematic method for the analysis of waveguides with arbitrarily shaped cross section is strongly recommended for computer-aided design and optimization of complex microwave systems, in which different guiding structures are involved. Although the finite element (or difference) method (e.g. [1] and [2]) and the mode-matching technique (e.g. [3] and [4]) are capable of analyzing a wide variety of structures, their storage and/or CPU time requirements represent severe restrictions on any economical CAD algorithm.

Many guiding structures simply have a rectangular or a circular outer boundary and one (or more) contacting or noncontacting metal inserts which may be either solid or sheetlike. Examples are striplines and microstrips, finned waveguides and finlines, ridge waveguides, and multiconductor transmission lines. The electromagnetic field inside these structures can be expanded in terms of the eigenmodes of the corresponding hollow rectangular or circular waveguide in such a way that the different expansions vanish everywhere inside the metal inserts. This procedure corresponds to the one-dimensional Fourier series, in which a function which vanishes over a certain interval can be expanded with respect to the harmonics corresponding to a larger interval which includes the smaller one.

Manuscript received February 28, 1989; revised June 26, 1989.

The authors are with the Arbeitsbereich Hochfrequenztechnik, Technische Universität Hamburg–Harburg, Postfach 90 14 03, D-2100 Hamburg 90, West Germany.

IEEE Log Number 8930809.

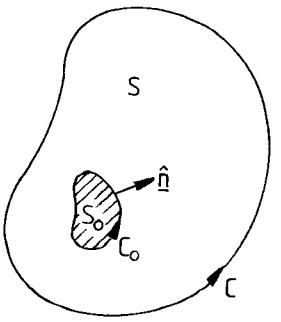

Fig. 1. Cross section of a waveguide with a metal insert.

In this paper, only homogeneously filled waveguides will be considered. If the method presented here is, however, combined with that presented in [5], inhomogeneously filled structures can be analyzed likewise.

II. Basic Formulation

Fig. 1 shows the cross section of a waveguide with a single contacting or noncontacting metal insert. Extending the analysis to multiconductor transmission lines is straightforward. The direction of propagation, in which the structure is uniform, is taken along the z axis with the corresponding propagation constant β. Let $\{h_{zn}\}$ and $\{e_{zn}\}$ be the complete sets of axial magnetic and electric fields which characterize the TE and TM modes, respectively, of the hollow waveguide (i.e., with the metal insert S_0 removed). Then h_{zn} and e_{zn} are real functions of the transverse coordinates, which correspond to the cutoff wavenumbers k_{nh} and k_{ne}, respectively, and satisfy the orthogonality relations [6]

$$\int_S h_{zn} h_{zm}\, dS = P_{nh}\delta_{nm} \tag{1a}$$

$$\int_S e_{zn} e_{zm}\, dS = P_{ne}\delta_{nm} \tag{1b}$$

where δ_{nm} is the Kronecker delta.

Let ∇_t and $\hat{\boldsymbol{k}}$ be the transverse component of the del operator and the unit vector in the axial direction, respectively. The set $\{\nabla_t e_{zn}\}$ is, in fact, complete with respect to the curl-free transverse electric fields, while the set $\{\hat{\boldsymbol{k}} \times \nabla_t h_{zn}\}$ is complete with respect to the divergence-free transverse electric fields. The two sets $\{\nabla_t h_{zn}\}$ and $\{\nabla_t e_{zn} \times \hat{\boldsymbol{k}}\}$ have the same properties with respect to transverse magnetic fields.

Let $\boldsymbol{e}$, $\boldsymbol{h}$, e_z, and h_z be the transverse electric, transverse magnetic, axial electric, and axial magnetic field, respec-

0018-9480/89/1200-1924$01.00 ©1989 IEEE

tively, in the original structure (i.e., with the metal insert S_0 present) with z dependence $e^{-j\beta z}$ being dropped out. Then

$$\nabla_t \times \boldsymbol{e} = -j\omega\mu_0 h_z \hat{\boldsymbol{k}} \tag{2a}$$

$$\nabla_t \times \boldsymbol{h} = j\omega\epsilon_0 e_z \hat{\boldsymbol{k}} \tag{2b}$$

$$\nabla_t h_z + j\beta \boldsymbol{h} = j\omega\epsilon_0 (\hat{\boldsymbol{k}} \times \boldsymbol{e}) \tag{2c}$$

$$\nabla_t e_z + j\beta \boldsymbol{e} = -j\omega\mu_0 (\hat{\boldsymbol{k}} \times \boldsymbol{h}). \tag{2d}$$

These field components can be expressed as expansions in terms of the above-mentioned complete sets. Because the expansions are defined everywhere over S, it must be claimed that they vanish identically over S_0. Then e_z, the tangential component of $\boldsymbol{e}$, and the normal component of $\boldsymbol{h}$, which must vanish on C_0, are continuous across C_0. On the other hand, h_z, the tangential component of $\boldsymbol{h}$, and the normal component of $\boldsymbol{e}$, which generally do not vanish on C_0, have step discontinuities at C_0.

Because the structure is homogeneously filled (empty), it can support either TE or TM modes (the TEM mode will be shown to be a TM mode with vanishing cutoff wavenumber).

A. TE Modes

Because the tangential component of $\boldsymbol{h}$ has a step discontinuity at C_0, $(\nabla_t \times \boldsymbol{h})$, which includes the normal derivative of the tangential component, behaves as a Dirac delta function there. This dirac delta function is just the axial component of the surface current at C_0. The vector $(\nabla_t \times \boldsymbol{h})$ can then vanish everywhere over S except at C_0, and hence $\boldsymbol{h}$ cannot be expanded in terms of the curl-free set $\{\nabla_t h_{zn}\}$ only. It needs, in addition, the divergence-free set $\{\nabla_t e_{zn} \times \hat{\boldsymbol{k}}\}$. The transverse components $\boldsymbol{h}$ and $\boldsymbol{e}$ can then be expanded as

$$\boldsymbol{h} = -j\beta \left[\sum_n \frac{a_n^{(h)}}{\sqrt{P_{nh}}} \nabla_t h_{zn} + \sum_n \frac{b_n^{(h)}}{\sqrt{P_{ne}}} (\nabla_t e_{zn} \times \hat{\boldsymbol{k}}) \right] \tag{3a}$$

$$\boldsymbol{e} = \frac{j\omega\mu_0}{j\beta} (\boldsymbol{h} \times \hat{\boldsymbol{k}}). \tag{3b}$$

Because the normal component of $\boldsymbol{h}$ is continuous across C_0, h_z can be obtained from $(j\beta h_z = \nabla_t \cdot \boldsymbol{h})$ by a term-by-term differentiation of (3a):

$$h_z = \sum_n \frac{a_n^{(h)}}{\sqrt{P_{nh}}} k_{nh}^2 h_{zn}. \tag{4}$$

The expansion coefficients $a_n^{(h)}$ and $b_n^{(h)}$ are obtained by making use of the orthogonality relations (1):

$$a_n^{(h)} = \frac{-1}{j\beta k_{nh}^2 \sqrt{P_{nh}}} \int_{S-S_0} \boldsymbol{h} \cdot \nabla_t h_{zn} \, dS \tag{5a}$$

$$b_n^{(h)} = \frac{-1}{j\beta k_{ne}^2 \sqrt{P_{ne}}} \int_{S-S_0} \boldsymbol{h} \cdot (\nabla_t e_{zn} \times \hat{\boldsymbol{k}}) \, dS. \tag{5b}$$

The integration is taken over $(S - S_0)$ in order to guarantee the vanishing of $\boldsymbol{h}$ and $\boldsymbol{e}$ given by (3) everywhere on S_0. After some mathematical manipulations, one obtains

$$a_n^{(h)} = \frac{1}{(k_{nh}^2 - k_c^2) k_{nh}^2 \sqrt{P_{nh}}} \oint_{C_0} h_z (\hat{\boldsymbol{n}} \cdot \nabla_t h_{zn}) \, dl \tag{6a}$$

$$b_n^{(h)} = \frac{1}{k_{ne}^2 k_c^2 \sqrt{P_{ne}}} \oint_{C_0} h_z ((\hat{\boldsymbol{n}} \times \hat{\boldsymbol{k}}) \cdot \nabla_t e_{zn}) \, dl \tag{6b}$$

where k_c is the cutoff wavenumber $(k_c^2 = k_0^2 - \beta^2)$.

B. TM Modes

Because the tangential component of $\boldsymbol{e}$ is continuous across C_0, $(\nabla_t \times \boldsymbol{e})$ is free from Dirac delta functions at C_0 and hence can vanish everywhere on S. Consequently, $\boldsymbol{e}$ can be expanded in terms of the curl-free set $\{\nabla_t e_{zn}\}$. The transverse components $\boldsymbol{e}$ and $\boldsymbol{h}$ can then be written as

$$\boldsymbol{e} = \sum_n \frac{a_n^{(e)}}{\sqrt{P_{ne}}} \nabla_t e_{zn} \tag{7a}$$

$$\boldsymbol{h} = \frac{j\omega\epsilon_0}{j\beta} (\hat{\boldsymbol{k}} \times \boldsymbol{e}). \tag{7b}$$

Because e_z is continuous across C_0, it can be obtained from $(-j\beta \nabla_t e_z = k_c^2 \boldsymbol{e})$ by a term-by term integration of (7a):

$$e_z = \frac{-k_c^2}{j\beta} \sum_n \frac{a_n^{(e)}}{\sqrt{P_{ne}}} e_{zn}. \tag{8}$$

Following a procedure similar to that for the TE modes, the expansion coefficients $a_n^{(e)}$ are obtained:

$$a_n^{(e)} = \frac{1}{(k_c^2 - k_{ne}^2) \sqrt{P_{ne}}} \oint_{C_0} e_{zn} (\hat{\boldsymbol{n}} \cdot \boldsymbol{e}) \, dl. \tag{9}$$

If $k_c = 0$, $e_z = 0$ and the TEM mode is obtained. The quantity $(j\beta e_z / k_c^2)$ is, however, finite and plays the same role as an electrostatic potential φ.

III. Matrix Formulation

If the contour C_0 is closed and smooth enough, i.e., free from sharp edges, the different field components are regular at C_0 so that their series representations converge rapidly. In this case, h_z in (6) and $(\hat{\boldsymbol{n}} \cdot \boldsymbol{e})$ in (9) can be replaced by *twice* their series representations (4) and (7a), respectively. The factor *two* is due to the step discontinuities of h_z and $(\hat{\boldsymbol{n}} \cdot \boldsymbol{e})$ at C_0. The series in (4) and (7a) converge then to only half the value of h_z and $(\hat{\boldsymbol{n}} \cdot \boldsymbol{e})$, respectively, at C_0.

Substituting (4) into (6a), one arrives at the following matrix eigenvalue equation for TE modes:

$$([\Lambda^h] - [C^h])[\Lambda^h] \boldsymbol{a}^{(h)} = k_c^2 [\Lambda^h] \boldsymbol{a}^{(h)} \tag{10}$$

where $[\Lambda^h]$ is a diagonal matrix with elements k_{nh}^2, and $\boldsymbol{a}^{(h)}$ is a column vector with elements $a_n^{(h)}$. The elements of

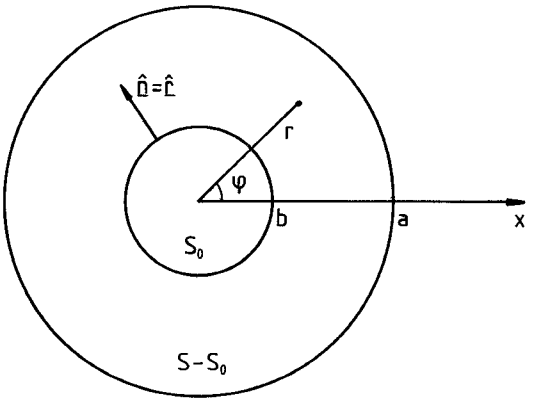

Fig. 2. Cross section of a coaxial transmission line.

the square matrix $[C^h]$ are given by

$$C_{nm}^h = \frac{2}{\sqrt{P_{nh}P_{mh}}} \oint_{C_0} h_{zm}(\hat{\boldsymbol{n}} \cdot \nabla_t h_{zn})\, dl. \tag{11}$$

Substituting (4) into (6b), the column vector $\boldsymbol{b}^{(h)}$ with elements $b_n^{(h)}$ is given by

$$\boldsymbol{b}^{(h)} = \frac{1}{k_c^2}[\Lambda^e]^{-1}[T][\Lambda^h]\boldsymbol{a}^{(h)} \tag{12}$$

where $[\Lambda^e]$ is a diagonal matrix with elements k_{ne}^2, and $[T]$ is, principally, a nonsquare matrix with elements given by

$$T_{nm} = \frac{2}{\sqrt{P_{ne}P_{mh}}} \oint_{C_0} h_{zm}\big((\hat{\boldsymbol{n}} \times \hat{\boldsymbol{k}}) \cdot \nabla_t e_{zn}\big)\, dl. \tag{13}$$

Substituting (7a) into (9), the following matrix eigenvalue equation is obtained for TM modes:

$$([\Lambda^e] + [C^e])\boldsymbol{a}^{(e)} = k_c^2 \boldsymbol{a}^{(e)} \tag{14}$$

where $\boldsymbol{a}^{(e)}$ is a column vector with elements $a_n^{(e)}$. The elements of the square matrix $[C^e]$ are now given by

$$C_{nm}^e = \frac{2}{\sqrt{P_{ne}P_{me}}} \oint_{C_0} e_{zn}(\hat{\boldsymbol{n}} \cdot \nabla_t e_{zm})\, dl. \tag{15}$$

It is worth noting that if we look for the dual field, which exists on S_0 and vanishes identically over $(S - S_0)$, the above analysis remains valid if the normal unit vector $\hat{\boldsymbol{n}}$ is replaced by $-\hat{\boldsymbol{n}}$ in all contour integrations. For the matrix formulation, this has the effect of changing only the signs of the matrices $[C^h]$, $[T]$, and $[C^e]$. Both dual cases can consequently be analyzed using the same equations if these sign changes are taken into account.

The matrix eigenvalue equations (10) and (14) have essentially doubly infinite order. For computational purposes, the series in (3), (4), (7), and (8) must be truncated, retaining a finite number of terms. The matrices in (10), (12), and (14) then become of finite order.

IV. Azimuthally Independent TM Modes in a Coaxial Line

In order to demonstrate the validity of the matrix formulation, a simple structure is analyzed: a coaxial line.

TABLE I
First Ten Eigenvalues Corresponding to Different Matrix Sizes for the Coaxial Case with $\alpha = 0.5$

Eigenvalue	1	2	3	4	5
(50x50)	0.2209	6.2373	12.5383	18.8278	25.1142
(100x100)	0.1567	6.2416	12.5425	18.8321	25.1185
(200x200)	0.1109	6.2438	12.5447	18.8343	25.1207
Exact	0.0000	6.2461	12.5469	18.8364	25.1228

Eigenvalue	6	7	8	9	10
(50x50)	31.3993	37.6837	43.9677	50.2514	56.5350
(100x100)	31.4037	37.6882	43.9723	50.2562	56.5399
(200x200)	31.4058	37.6903	43.9745	50.2584	56.5421
Exact	31.4080	37.6925	43.9766	50.2605	56.5443

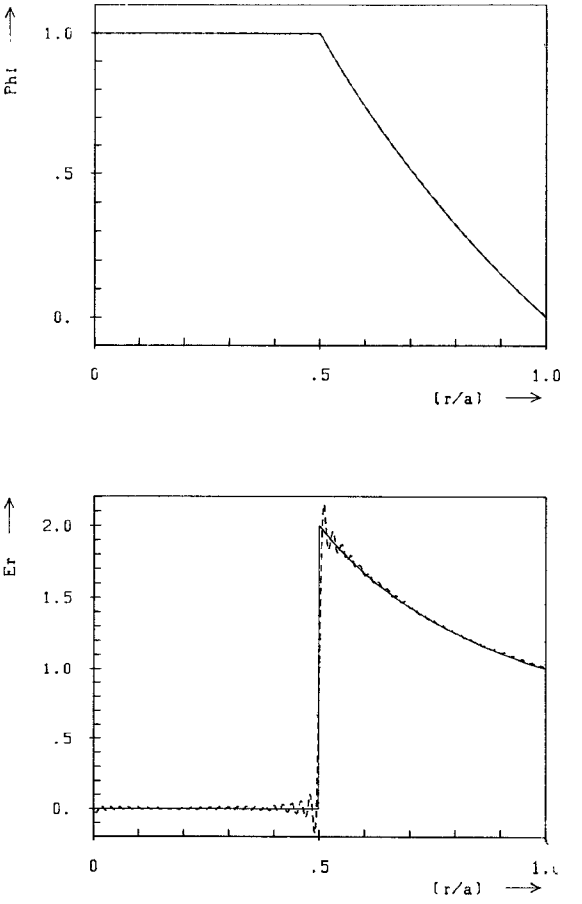

Fig. 3. Electrostatic potential and radial electric field for the coaxial case with $\alpha = 0.5$----- matrix formulation; ——— exact.

The TEM dominant mode is one of the TM modes, which corresponds to $k_c = 0$. Due to the rotational symmetry, the modes with different azimuthal dependences are decoupled. For illustration, only azimuthally independent TM modes are considered. Fig. 2 shows the cross section of a coaxial transmission line with outer and inner conductor radii a and b, respectively. The φ-independent set $\{e_{zn}\}$ is

TABLE II
FIRST TEN EIGENVALUES CORRESPONDING TO DIFFERENT MATRIX SIZES FOR THE CIRCULAR WAVEGUIDE CASE WITH $\alpha = 0.5$

Eigenvalue	1	2	3	4	5
(50x50)	4.8007	11.0313	17.2986	23.5742	29.8529
(100x100)	4.8052	11.0358	17.3031	23.5787	29.8575
(200x200)	4.8074	11.0380	17.3053	23.5809	29.8597
Exact	4.8097	11.0402	17.3075	23.5831	29.8618

Eigenvalue	6	7	8	9	10
(50x50)	36.1331	42.4141	48.6956	54.9775	61.2595
(100x100)	36.1378	42.4189	48.7006	54.9825	61.2648
(200x200)	36.1400	42.4211	48.7028	54.9848	61.2670
Exact	36.1421	42.4233	48.7049	54.9870	61.2692

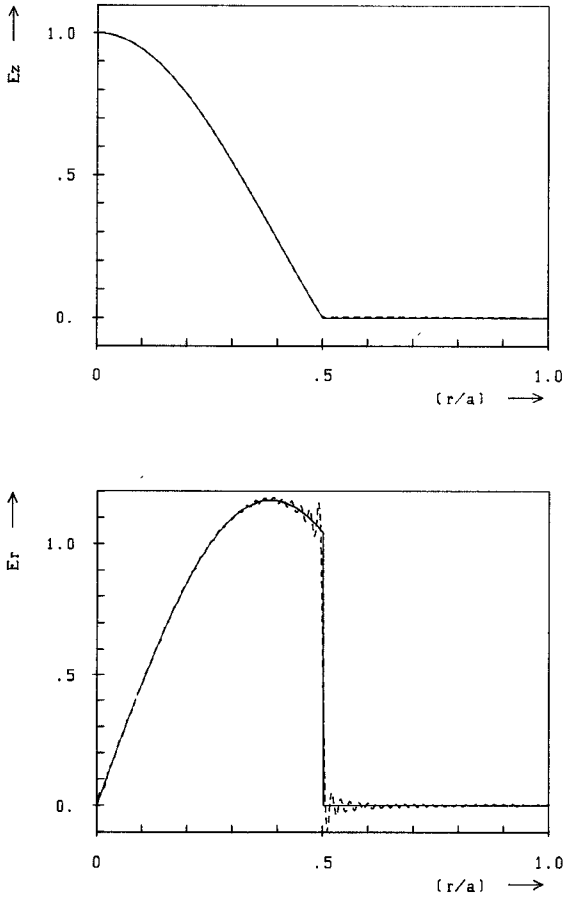

Fig. 4. Axial and radial electric fields for the circular waveguide case with $\alpha = 0.5$. ----- matrix formulation; ——— exact.

characterized by

$$e_{zn} = J_0(k_{ne} r) \tag{16a}$$

$$k_{ne} = \frac{p_n}{a} \tag{16b}$$

$$P_{ne} = \pi a^2 J_1^2(p_n) \tag{16c}$$

$$n = 1, 2, 3, \ldots \tag{16d}$$

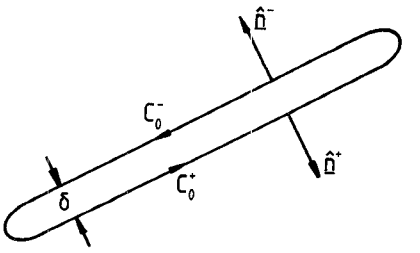

Fig. 5. Thin metal insert.

where $J_0(x)$ and $J_1(x)$ are Bessel functions of the first kind and zeroth and first order, respectively, and p_n is the nth zero of $J_0(x)$. Substituting (16) into (15), one arrives at

$$C^e_{nm} = \frac{-4\alpha p_m J_0(p_n\alpha) J_1(p_m\alpha)}{a^2 J_1(p_n) J_1(p_m)} \tag{17}$$

where $\alpha = b/a$. Referring to (14), the different eigenvalues of $([\Lambda^e] \pm [C^e])$ are numerically calculated. The positive sign refers to fields which exist in the coaxial region and vanish over the inner conductor, while the negative sign refers to the dual fields.

These two cases will be referred to as the coaxial case and the circular waveguide case, respectively. Table I shows the first ten eigenvalues corresponding to different matrix sizes for the coaxial case with $\alpha = 0.5$. Exact values are also included for comparison. The field corresponding to the smallest eigenvalue is plotted in Fig. 3 along with the exact field. It represents the electrostatic potential φ and the radial electric field e_r in the coaxial region. The same is demonstrated by Table II and Fig. 4 for the dual case, namely the circular waveguide case.

V. MOMENT METHOD FORMULATION

If the contour C_0 has sharp edges, some field components become singular at these edges. A large number of terms must then be retained in the series representing these components, which results in oversized matrices in (10) and (14). Another case, for which the matrix formulation is not valid at all, is when the contour C_0 is open; i.e., the metal insert is idealized to an infinitesimally thin one. Referring to Fig. 5, as $\delta \to 0$, $C_0^- \to C_0^+$, $\hat{n}^- \to -\hat{n}^+$. The other fields involved in (11), (13), and (15) are continuous everywhere on S and hence the matrices $[C^h]$, $[T]$, and $[C^e]$ will vanish as $\delta \to 0$.

When (6) and (9) are, however, investigated in the limiting case $\delta = 0$, it is easily shown that the contour integral along C_0 can be replaced by a simple line integral along C_0^+ if $\hat{n}$ is replaced by $\hat{n}^+$, and h_z and $(\hat{n} \cdot e)$ are replaced by $(h_z^+ - h_z^-)$ and $(\hat{n}^+ \cdot e^+ - \hat{n}^+ \cdot e^-)$, respectively. This procedure corresponds to the fact that the surface currents (charges) at C_0^+ and C_0^- will add together, forming a single current (charge) sheet if $\delta = 0$. In the following, no special symbols will be used for this case. The usual symbols must be interpreted according to the above discussion.

For the above-mentioned cases, it is more suitable to expand h_z and $(\hat{n} \cdot e)$ at C_0 in terms of basis functions,

which individually satisfy the edge conditions

$$h_z|_{C_0} = \sum_i I_i \eta_i \tag{18a}$$

$$(\hat{\boldsymbol{n}} \cdot \boldsymbol{e})|_{C_0} = \sum_i V_i \xi_i. \tag{18b}$$

Here I_i and V_i are expansion coefficients, and η_i and ξ_i are the basis functions. The expansion coefficients are determined by asking for a vanishing tangential electric field (or normal magnetic field) at C_0. If we test the vanishing fields at C_0 by the same basis functions (Galerkin's procedure), we arrive at the following equations:

$$\boldsymbol{a}^{(h)} = [\Lambda^h]^{-1/2}\left([\Lambda^h] - k_c^2[I]\right)^{-1}[\tilde{C}^{hh}]\boldsymbol{I} \tag{19a}$$

$$\boldsymbol{b}^{(h)} = \frac{1}{k_c^2}[\Lambda^e]^{-1/2}[\tilde{C}^{he}]\boldsymbol{I} \tag{19b}$$

$$\left\{k_c^2[\tilde{C}^{hh}]^t\left(k_c^2[I] - [\Lambda^h]\right)^{-1}[\tilde{C}^{hh}] + [\tilde{C}^{he}]^t[\tilde{C}^{he}]\right\}\boldsymbol{I} = 0 \tag{19c}$$

for TE modes, and

$$\boldsymbol{a}^{(e)} = \left(k_c^2[I] - [\Lambda^e]\right)^{-1}[\tilde{C}^{ee}]\boldsymbol{V} \tag{20a}$$

$$[\tilde{C}^{ee}]^t\left(k_c^2[I] - [\Lambda^e]\right)^{-1}[\tilde{C}^{ee}]\boldsymbol{V} = 0 \tag{20b}$$

for TM modes. $\boldsymbol{I}$ and $\boldsymbol{V}$ are column vectors with elements I_i and V_i, respectively, $[I]$ is the identity matrix, and $[\tilde{C}^{hh}]^t$, $[\tilde{C}^{he}]^t$, and $[\tilde{C}^{ee}]^t$ are the transposes of $[\tilde{C}^{hh}]$, $[\tilde{C}^{he}]$, and $[\tilde{C}^{ee}]$, respectively. The elements of the latter matrices are given by

$$\tilde{C}_{ni}^{hh} = \frac{1}{k_{nh}\sqrt{P_{nh}}}\oint_{C_0} \eta_i(\hat{\boldsymbol{n}} \cdot \nabla_t h_{zn})\, dl \tag{21a}$$

$$\tilde{C}_{ni}^{he} = \frac{1}{k_{ne}\sqrt{P_{ne}}}\oint_{C_0} \eta_i\left((\hat{\boldsymbol{n}} \times \hat{\boldsymbol{k}}) \cdot \nabla_t e_{zn}\right) dl \tag{21b}$$

$$\tilde{C}_{ni}^{ee} = \frac{1}{\sqrt{P_{ne}}}\oint_{C_0} \xi_i e_{zn}\, dl. \tag{21c}$$

It is worth noting that the characteristic equations (19c) and (20b) are valid for the already defined dual fields. Similar to the argument used in the matrix formulation, it is easily shown that the difference between the two dual fields is a sign change for the matrices $[\tilde{C}^{hh}]$, $[\tilde{C}^{he}]$, and $[\tilde{C}^{ee}]$, which enter the characteristic equations (19c) and (20b) along with their transpose matrices. The sign changes are consequently eliminated and the characteristic equations are valid for both dual fields.

The size of the characteristic matrix in (19c) and (20b) is equal to the number of basis functions used, which can be greatly reduced if the basis functions are properly chosen. On the other hand, each matrix element is a doubly infinite sum (over the subscript n), which must be truncated if it is not expressible in closed form. The truncation limit can, however, be put sufficiently high in order to correctly account for the singular behavior of certain field components at the edges. In this procedure the truncation limit does not influence the size of the characteristic matrix.

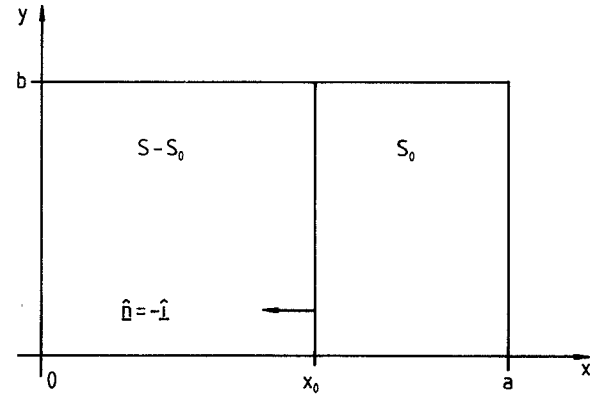

Fig. 6. Rectangular waveguide bifurcation.

The moment method formulation is basically the same as that presented in [7], except for the form of Green's functions used. In [7], the singular parts of the Green's functions have explicitly been written as logarithmic functions. The singularity is then removed by integration when the actual field is calculated. In this formulation, the fields themselves and not Green's functions are used. No singularity is then included, and all series converge uniformly.

VI. Application to Waveguide Bifurcations

The validity of the moment method formulation is demonstrated by investigating some special cases, for which the distribution of the unknown fields on C_0 (i.e., h_z for TE modes and $(\hat{\boldsymbol{n}} \cdot \boldsymbol{e})$ for TM modes) is known. Only one basis function, which is proportional to the known distribution, can consequently lead to the exact solution.

A. y-Independent TE Modes in a Rectangular Waveguide Bifurcation

Consider the rectangular waveguide with metal sheet at $x = x_0$ which is shown in Fig. 6. Because the structure is uniform in the y direction, modes with different y dependences are decoupled. For simplicity y-independent TE modes are considered. As $\{e_{zn}\}$ must be y-dependent, $\boldsymbol{b}^{(h)} = 0$, and only $\{h_{zn}\}$ is necessary for the field expansion. Another explanation for the absence of $\{e_{zn}\}$ is the absence of a y-independent axial surface current on the metal sheet at $x = x_0$, which means that the transverse magnetic field $\boldsymbol{h}$ is curl-free everywhere. The set $\{h_{zn}\}$ is characterized by

$$h_{zn} = \cos\frac{n\pi x}{a} \tag{22a}$$

$$k_{nh} = \frac{n\pi}{a} \tag{22b}$$

$$P_{nh} = \frac{ab}{2} \tag{22c}$$

$$n = 1, 2, 3 \cdots \tag{22d}$$

For y-independent modes, the following choice of the basis functions in (18a) leads to the exact solution:

$$\eta_i = \begin{cases} 1 & \text{if } i = 1 \\ 0 & \text{if } i \neq 1 \end{cases} \tag{23a}$$

and hence

$$h_z|_{x=x_0} = I_1 \quad \text{(constant)}. \tag{23b}$$

The elements of $[\tilde{C}^{hh}]$ in (21a) are then given by

$$\tilde{C}^{hh}_{ni} = \begin{cases} \sqrt{\dfrac{2b}{a}} \sin n\varphi_0 & \text{if } i=1 \\ 0 & \text{if } i \neq 1 \end{cases} \tag{24}$$

where $\varphi_0 = \pi x_0/a$. The field expansion coefficients $a_n^{(h)}$ in (19a) are hence expressed as

$$a_n^{(h)} = \sqrt{\frac{2b}{a}} \left(\frac{a}{\pi}\right)^3 \frac{\sin n\varphi_0}{n\left(n^2 - \bar{k}_c^2\right)} I_1 \tag{25}$$

where $\bar{k}_c = k_c a/\pi$. Substituting (22) and (25) into (4), one arrives at

$$h_z = \frac{I_1}{\pi} \sum_{n=1}^{\infty} \frac{n\left(\sin n(\varphi_0+\varphi) + \sin n(\varphi_0-\varphi)\right)}{\left(n^2 - \bar{k}_c^2\right)} \tag{26a}$$

where $\varphi = \pi x/a$. On the other hand, the characteristic equation (19c) reads

$$I_1 \sum_{n=1}^{\infty} \frac{\sin^2 n\varphi_0}{\left(n^2 - \bar{k}_c^2\right)} = 0. \tag{26b}$$

The two infinite series in (26) have closed-form expressions (see e.g. [8]), which are given by

$$h_z = \frac{I_1}{\sin \bar{k}_c \pi} \begin{cases} \sin \bar{k}_c(\pi - \varphi_0)\cos \bar{k}_c \varphi & \text{if } \varphi < \varphi_0 \\ -\sin \bar{k}_c \varphi_0 \cos \bar{k}_c(\pi - \varphi) & \text{if } \varphi > \varphi_0 \end{cases} \tag{27a}$$

$$\frac{I_1}{\bar{k}_c \sin \bar{k}_c \pi} \sin \bar{k}_c \varphi_0 \sin \bar{k}_c(\pi - \varphi_0) = 0. \tag{27b}$$

There are two possible solutions for (27b). Either $\sin \bar{k}_c \varphi_0 = 0$ and hence h_z and all field components vanish identically for $\varphi_0 < \varphi \leqslant \pi$, or $\sin \bar{k}_c(\pi - \varphi_0) = 0$ and hence h_z and all field components vanish identically for $0 \leqslant \varphi < \varphi_0$. These solutions characterize the already defined dual fields. They represent the y-independent TE modes in the two complementary regions $0 \leqslant \varphi < \varphi_0$ and $\varphi_0 < \varphi \leqslant \pi$, respectively.

B. φ-Independent TM Modes in a Circular Waveguide Bifurcation

A circular waveguide bifurcation represents a coaxial transmission line with a hollow inter conductor. The cross section of the structure is shown in Fig. 2. The φ-independent TM modes are expressed in terms of $\{e_{zn}\}$, which has been described in (16). The basis functions in (18b), which lead to the exact solution, are given by

$$\xi_i = \begin{cases} 1 & \text{if } i=1 \\ 0 & \text{if } i \neq 1. \end{cases} \tag{28a}$$

The normal electric field at $r = b$ is then given by

$$(\hat{\boldsymbol{n}} \cdot \boldsymbol{e})|_{r=b} = e_r|_{r=b} = V_1 \quad \text{(constant)}. \tag{28b}$$

Equation (21c) then reads

$$\tilde{C}^{ee}_{ni} = \begin{cases} \dfrac{2\sqrt{\pi}\,\alpha J_0(p_n\alpha)}{J_1(p_n)} & \text{if } i=1 \\ 0 & \text{if } i \neq 1. \end{cases} \tag{29}$$

The field expansion coefficients $a_n^{(e)}$ in (20a) are then given by

$$a_n^{(e)} = \frac{2\sqrt{\pi}\,\alpha a^2 J_0(p_n\alpha)}{J_1(p_n)\left(\tilde{k}_c^2 - p_n^2\right)} V_1 \tag{30}$$

where $\tilde{k}_c = k_c a$. Substituting (16) and (30) into (8), one arrives at

$$-\frac{j\beta}{k_c^2} e_z = 2\alpha a V_1 \sum_{n=1}^{\infty} \frac{J_0(p_n\alpha) J_0(p_n\tilde{r})}{J_1(p_n)\left(\tilde{k}_c^2 - p_n^2\right)} \tag{31a}$$

where $\tilde{r} = r/a$. The characteristic equation (20b) is reduced to

$$V_1 \sum_{n=1}^{\infty} \frac{J_0^2(p_n\alpha)}{J_1^2(p_n)\left(\tilde{k}_c^2 - p_n^2\right)} = 0. \tag{31b}$$

Again the two infinite series in (31) have closed-form expressions [8] which read

$$\frac{-j\beta}{k_c^2} e_z = \frac{\pi\alpha a}{2J_0(\tilde{k}_c)} V_1 \begin{cases} J_0(\tilde{k}_c\tilde{r})\left[J_0(\tilde{k}_c)Y_0(\tilde{k}_c\alpha) - J_0(\tilde{k}_c\alpha)Y_0(\tilde{k}_c)\right] & \text{if } \tilde{r} \leqslant \alpha \\ J_0(\tilde{k}_c\alpha)\left[J_0(\tilde{k}_c)Y_0(\tilde{k}_c\tilde{r}) - J_0(\tilde{k}_c\tilde{r})Y_0(\tilde{k}_c)\right] & \text{if } \tilde{r} \geqslant \alpha \end{cases} \tag{32a}$$

$$\frac{V_1}{J_0(\tilde{k}_c)} J_0(\tilde{k}_c\alpha)\left[J_0(\tilde{k}_c)Y_0(\tilde{k}_c\alpha) - J_0(\tilde{k}_c\alpha)Y_0(\tilde{k}_c)\right] = 0 \tag{32b}$$

where $Y_0(x)$ means the Bessel function of the second kind and zeroth order. There are again two possible solutions. Either $J_0(\tilde{k}_c\alpha) = 0$ or $J_0(\tilde{k}_c)Y_0(\tilde{k}_c\alpha) = J_0(\tilde{k}_c\alpha)Y_0(\tilde{k}_c)$. The first solution represents a field which exists within the inner conductor ($0 \leqslant r < b$) and vanishes on the coaxial region ($b < r \leqslant a$). The second solution represents the dual field.

VII. Application to Stripline and Ridge Waveguide

The moment method formulation is now applied to two other cases, for which closed-form expressions cannot be obtained.

A. TE Modes on a Stripline

Consider the stripline with the cross section shown in Fig. 7. The sets $\{h_{zn}\}$ and $\{e_{zn}\}$ are two-dimensional so the subscript n must be replaced by nm. The two sets are

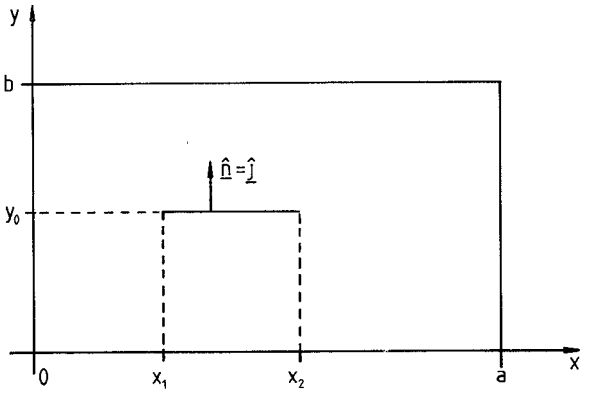

Fig 7. Cross section of a stripline.

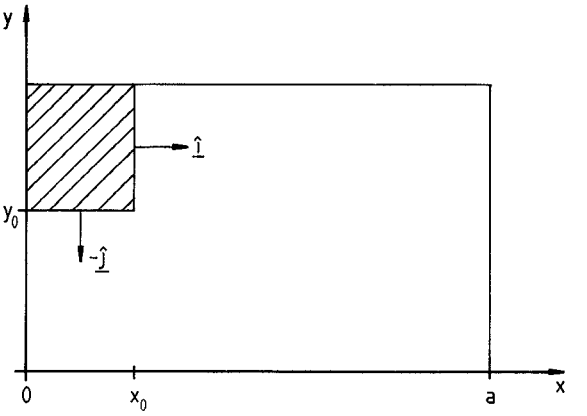

Fig. 8. Cross section of a ridge waveguide.

described by

$$h_{znm} = \cos\frac{n\pi x}{a}\cos\frac{m\pi y}{b} \tag{33a}$$

$$n = 0,1,2,\cdots, \qquad m = 0,1,2,\cdots,$$

$$(n,m) \neq (0,0) \tag{33b}$$

$$e_{znm} = \sin\frac{n\pi x}{a}\sin\frac{m\pi y}{b} \tag{33c}$$

$$n = 1,2,3,\cdots, \qquad m = 1,2,3,\cdots \tag{33d}$$

$$k_{nmh}^2 = k_{nme}^2 = k_{nm}^2 = \left(\frac{n\pi}{a}\right)^2 + \left(\frac{m\pi}{b}\right)^2 \tag{33e}$$

$$P_{nmh} = P_{nme} = P_{nm} = \frac{ab}{4}(1+\delta_{n0})(1+\delta_{m0}). \tag{33f}$$

The discontinuity in the axial magnetic field is expanded according to

$$h_z^+ - h_z^-|_{y=y_0} = \sum_t I_t \eta_t(x). \tag{34}$$

In order to reduce the order of the characteristic matrix in (19c), the basis functions $\eta_t(x)$ should satisfy the 0°-edge conditions at $x = x_1$ and $x = x_2$; i.e., they should behave like $|x - x_i|^{1/2}$ *as* $x \to x_i$, $i = 1,2$,[9]. Equations (21a) and (21b) are then reduced to

$$\tilde{C}_{nmi}^{hh} = -\frac{m\pi}{2}\frac{a(1+\delta_{n0})}{b}\frac{\sin m\psi_0}{k_{nm}\sqrt{P_{nm}}}\tilde{\eta}_{in} \tag{35a}$$

$$\tilde{C}_{nmi}^{he} = \frac{n\pi}{2}\frac{\sin m\psi_0}{k_{nm}\sqrt{P_{nm}}}\tilde{\eta}_{in} \tag{35b}$$

respectively, where

$$\tilde{\eta}_{in} = \frac{2}{a(1+\delta_{n0})}\int_{x_1}^{x_2}\eta_i(x)\cos\frac{n\pi x}{a}dx \tag{36}$$

and $\psi_0 = \pi y_0/b$. The characteristic equation (19c) can be written as

$$[Z]\boldsymbol{I} = 0 \tag{37a}$$

where

$$Z_{ij} = \sum_{n=0}^{\infty}\sum_{m=1}^{\infty} k_c^2 \frac{\tilde{C}_{nmi}^{hh}\tilde{C}_{nmj}^{hh}}{k_c^2 - k_{nm}^2} + \sum_{n=1}^{\infty}\sum_{m=1}^{\infty}\tilde{C}_{nmi}^{he}\tilde{C}_{nmj}^{he}. \tag{37b}$$

If (33) and (35) are substituted into (37b), it is readily shown that the sum over m can be expressed in closed form [8]. Equation (37b) is then reduced to

$$Z_{ij} = \frac{-\pi a}{2b}\sum_{n=0}^{\infty}(1+\delta_{n0})\bar{\alpha}_n\frac{\sin\bar{\alpha}_n\psi_0\sin\bar{\alpha}_n(\pi-\psi_0)}{\sin\bar{\alpha}_n\pi}\tilde{\eta}_{in}\tilde{\eta}_{jn} \tag{37c}$$

where

$$\bar{\alpha}_n = \frac{b}{\pi}\sqrt{k_c^2 - \left(\frac{n\pi}{a}\right)^2}. \tag{38}$$

The elements of $[Z]$, given by (37c), are easily shown to correspond to those that can be obtained by applying the standard spectral-domain technique (e.g. [10]). The moment method formulation for this case is then reduced to the well-known spectral-domain technique.

B. TM Modes in a Ridge Waveguide

Consider the ridge waveguide shown in Fig. 8. For simplicity, only the case with electric wall symmetry at $x = 0$ will be analyzed. The set $\{e_{zn}\}$ again is two-dimensional and identical to that described in (33). The normal electric field at the ridge is expanded as

$$(\hat{\boldsymbol{n}}\cdot\boldsymbol{e})|_{C_0} = \begin{cases} -e_y|_{y=y_0} = \sum_i V_i^{(1)}\xi_i^{(1)}(x), & 0 \leq x \leq x_0 \\ +e_x|_{x=x_0} = \sum_i V_i^{(2)}\xi_i^{(2)}(y), & y_0 \leq y \leq b. \end{cases} \tag{39}$$

To reduce the size of the characteristic matrix in (20b), the basis functions $\xi_i^{(1)}(x)$ and $\xi_i^{(2)}(y)$ should satisfy the 90°-edge conditions at (x_0, y_0); i.e., they should behave like $|x - x_0|^{-1/3}$ and $|y - y_0|^{-1/3}$ as $x \to x_0$ and $y \to y_0$, respectively [9].

In order to systematize the analysis, V and $[\tilde{C}^{ee}]$ in (20b) are written as

$$V = \begin{bmatrix} V^{(1)} \\ V^{(2)} \end{bmatrix} \tag{39a}$$

$$[\tilde{C}^{ee}] = [[\tilde{C}^{(1)}][\tilde{C}^{(2)}]] \tag{39b}$$

where $V^{(1)}$ and $V^{(2)}$ are column vectors with elements $V_i^{(1)}$ and $V_i^{(2)}$, respectively. The elements of $[\tilde{C}^{(1)}]$ and $[\tilde{C}^{(2)}]$ are given according to (21c) with ξ_i replaced by $\xi_i^{(1)}$ and $\xi_i^{(2)}$, respectively, i.e.,

$$\tilde{C}_{nmi}^{(1)} = \sqrt{\frac{a}{b}} \sin m\psi_0 \tilde{\xi}_{in}^{(1)} \tag{40a}$$

$$\tilde{C}_{nmi}^{(2)} = \sqrt{\frac{b}{a}} \sin n\varphi_0 \tilde{\xi}_{im}^{(2)} \tag{40b}$$

where

$$\tilde{\xi}_{in}^{(1)} = \frac{2}{a}\int_0^{x_0} \xi_i^{(1)}(x) \sin\frac{n\pi x}{a}\, dx \tag{41a}$$

$$\tilde{\xi}_{im}^{(2)} = \frac{2}{b}\int_{y_0}^{b} \xi_i^{(2)}(y) \sin\frac{m\pi y}{b}\, dy \tag{41b}$$

$\varphi_0 = \pi x_0/a$ and $\psi_0 = \pi y_0/b$. The characteristic equation (20b) is then reduced to

$$\begin{bmatrix} [Y^{(11)}] & [Y^{(12)}] \\ [Y^{(21)}] & [Y^{(22)}] \end{bmatrix} \begin{bmatrix} V^{(1)} \\ V^{(2)} \end{bmatrix} = 0 \tag{42}$$

with

$$Y_{ij}^{(11)} = \sum_{n=1}^{\infty}\sum_{m=1}^{\infty} \frac{\tilde{C}_{nmi}^{(1)}\tilde{C}_{nmj}^{(1)}}{k_c^2 - k_{nm}^2} \tag{43a}$$

$$Y_{ij}^{(12)} = \sum_{n=1}^{\infty}\sum_{m=1}^{\infty} \frac{\tilde{C}_{nmi}^{(1)}\tilde{C}_{nmj}^{(2)}}{k_c^2 - k_{nm}^2} \tag{43b}$$

$$Y_{ij}^{(21)} = Y_{ji}^{(12)} \tag{43c}$$

$$Y_{ij}^{(22)} = \sum_{n=1}^{\infty}\sum_{m=1}^{\infty} \frac{\tilde{C}_{nmi}^{(2)}\tilde{C}_{nmj}^{(2)}}{k_c^2 - k_{nm}^2}. \tag{43d}$$

It can easily be shown that one of the two sums in equations (43) can be expressed in closed form [8]. The other sum must be computed numerically. After some straightforward mathematical manipulation, (43) is reduced to

$$Y_{ij}^{(11)} = \frac{-ab}{2\pi}\sum_{n=1}^{\infty} \frac{\sin\bar{\alpha}_n(\pi-\psi_0)\sin\bar{\alpha}_n\psi_0}{\bar{\alpha}_n \sin\bar{\alpha}_n\pi} \tilde{\xi}_{in}^{(1)}\tilde{\xi}_{jn}^{(1)} \tag{44a}$$

$$Y_{ij}^{(12)} = Y_{ji}^{(21)}$$

$$= \frac{-b^2}{2\pi}\sum_{n=1}^{\infty} \frac{\sin n\varphi_0 \sin\bar{\alpha}_n\psi_0}{\bar{\alpha}_n \sin\bar{\alpha}_n\pi} \tilde{\xi}_{in}^{(1)}\tilde{\xi}_{jn}^{(2)}$$

$$= \frac{-a^2}{2\pi}\sum_{m=1}^{\infty} \frac{\sin m\psi_0 \sin\bar{\gamma}_m(\pi-\varphi_0)}{\bar{\gamma}_m \sin\bar{\gamma}_m\pi} \tilde{\xi}_{im}^{(1)}\tilde{\xi}_{jm}^{(2)} \tag{44b}$$

$$Y_{ij}^{(22)} = \frac{-ab}{2\pi}\sum_{m=1}^{\infty} \frac{\sin\bar{\gamma}_m(\pi-\varphi_0)\sin\bar{\gamma}_m\varphi_0}{\bar{\gamma}_m \sin\bar{\gamma}_m\pi} \tilde{\xi}_{im}^{(2)}\tilde{\xi}_{jm}^{(2)} \tag{44c}$$

with

$$\alpha_n = \sqrt{k_c^2 - \left(\frac{n\pi}{a}\right)^2} \qquad \bar{\alpha}_n = \frac{b}{\pi}\alpha_n \tag{45a}$$

$$\gamma_m = \sqrt{k_c^2 - \left(\frac{m\pi}{b}\right)^2} \qquad \bar{\gamma}_m = \frac{a}{\pi}\gamma_m \tag{45b}$$

$$\tilde{\xi}_{im}^{(1)} = \frac{2}{a}\int_0^{x_0} \xi_i^{(1)}(x) \sin\gamma_m x\, dx \tag{45c}$$

$$\tilde{\xi}_{in}^{(2)} = \frac{2}{b}\int_{y_0}^{b} \xi_i^{(2)}(y) \sin\alpha_n(b-y)\, dy. \tag{45d}$$

Referring to, e.g., [10], it is easily seen that $[Y^{(11)}]$ is the characteristic matrix of a corresponding structure with a single, infinitesimally thin strip at $y = y_0$, which extends from $x = 0$ to $x = x_0$, while $[Y^{(22)}]$ is the characteristic matrix of a corresponding structure with a single strip at $x = x_0$, which extends from $y = y_0$ to $y = b$. The elements of $[Y^{(12)}]$ are obtained from the elements of $[Y^{(11)}]$ by replacing $(a \sin\bar{\alpha}_n(\pi - \psi_0)\tilde{\xi}_{jn}^{(1)})$ by $(b \sin n\varphi_0 \tilde{\tilde{\xi}}_{jn}^{(2)})$.

The formulation presented here consequently is a generalization of the spectral-domain technique in that the finite metallization thickness is correctly taken into account. Any existing routine for the analysis of planar structures which is based on the spectral-domain technique can hence be modified according to the above statements in order to extend its validity to comprehend finite metallization thickness.

References

[1] P. Silvester, *Finite Elements for Electrical Engineers*. New York: Cambridge University Press, 1983.

[2] P. Daly, "Hybrid-mode analysis of microstrip by finite element method," *IEEE Trans. Microwave Theory Tech.*, vol. MTT-19, pp. 19–25, 1971.

[3] R. Vahldieck, "Accurate hybrid-mode analysis of various finline configurations including multilayered dielectrics, finite metallization thickness, and substrate holding grooves," *IEEE Trans. Microwave Theory Tech.*, vol. MTT-32, pp. 1454–1460, 1984.

[4] J. Bornemann, "Rigorous field theory analysis of quasiplanar waveguides," *Proc. Inst. Elec. Eng.*, pt. H, vol 132, pp. 1–5, 1985.

[5] A. S. Omar and K. Schünemann, "Complex and backward-wave modes in inhomogeneously and anisotropically filled waveguides," *IEEE Trans. Microwave Theory Tech.*, vol. MTT-35, pp. 268–275, 1987.

[6] R. E. Collin, *Field Theory of Guided Waves*. New York: McGraw-Hill, 1960.

[7] G. Conciauro, M. Bressan, and C. Zuffada, "Waveguide modes via an integral equation leading to a linear matrix eigenvalue problem," *IEEE Trans. Microwave Theory Tech.*, vol. MTT-32, pp. 1495–1504, 1984.

[8] F. Oberhettinger, *Fourier Expansions*. New York: Academic Press, 1973.

[9] R. Mittra and S. W. Lee, *Analytical Techniques in the Theory of Guided Waves*. New York: Macmillan, 1971.

[10] L.-P. Schmidt and T. Itoh, "Spectral domain analysis of dominant and higher order modes in fin-lines," *IEEE Trans. Microwave Theory Tech.*, vol. MTT-28, pp. 981–985, 1980.

Abbas S. Omar (M'86-SM'89) received the B.Sc. and M.Sc. degrees in electrical engineering from Ain Shams University, Cairo, Egypt, in 1978 and 1982, respectively, and the Doktor-Ing. degree from the Technische Universität Hamburg-Harburg, West Germany, in 1986.

From 1978 to 1982, he served as a Research and Teaching Assistant in the Department of Electronics and Computer Engineering of Ain Shams University, where he was engaged in investigations of microstrip lines and below-cutoff waveguides and their use in a hybrid circuit technique for the realization of broad-band tunable oscillators. From 1982 to 1983, he was with the Institut für Hochfrequenztechnik, Technische Universität Braunschweig, West Germany, as a Research Engineer, where he was involved with theoretical investigations of finlines. From 1983 to 1987 he held the same position at the Technische Universität Hamburg-Harburg, West Germany, where he was engaged in investigations of planar structures and dielectric resonators. Since then he has been a Senior Research Engineer at the Technische Universität Braunschweig, West Germany. His current fields of research are concerned with optimization of microwave ovens, the field analysis of dielectric resonators, the analysis and design of three-dimensional passive systems, theoretical investigations of guiding structures, and the design and optimization of planar structures.

✠

Klaus F. Schünemann (M'76-SM'86) was born in Braunschweig, West Germany, in 1939. He received the Dipl.-Ing. degree in electrical engineering and the Doktor-Ing. degree from the Technische Universität Braunschweig, West Germany, in 1965 and 1970, respectively.

Since 1983, he has been a Professor of Electrical Engineering and Director of the Arbeitsbereich Hochfrequenztechnik at the Technische Universität Hamburg-Harburg, West Germany. He has worked on nonlinear microwave circuits, diode modeling, solid-state oscillators, PCM communication systems, and integrated-circuit technologies such as finline and waveguide below cutoff. His current research interest are concerned with transport phenomena in submicron devices, CAD of planar millimeter-wave circuits, optoelectronics, and high-power millimeter-wave tubes.